Structure, Volume *25*

Supplemental Information

A Structural Model for Vinculin Insertion into PIP_2-Containing Membranes and the Effect of Insertion on Vinculin Activation and Localization

Peter M. Thompson, Srinivas Ramachandran, Lindsay B. Case, Caitlin E. Tolbert, Arpit Tandon, Mihir Pershad, Nikolay V. Dokholyan, Clare M. Waterman, and Sharon L. Campbell

Supplemental Figures

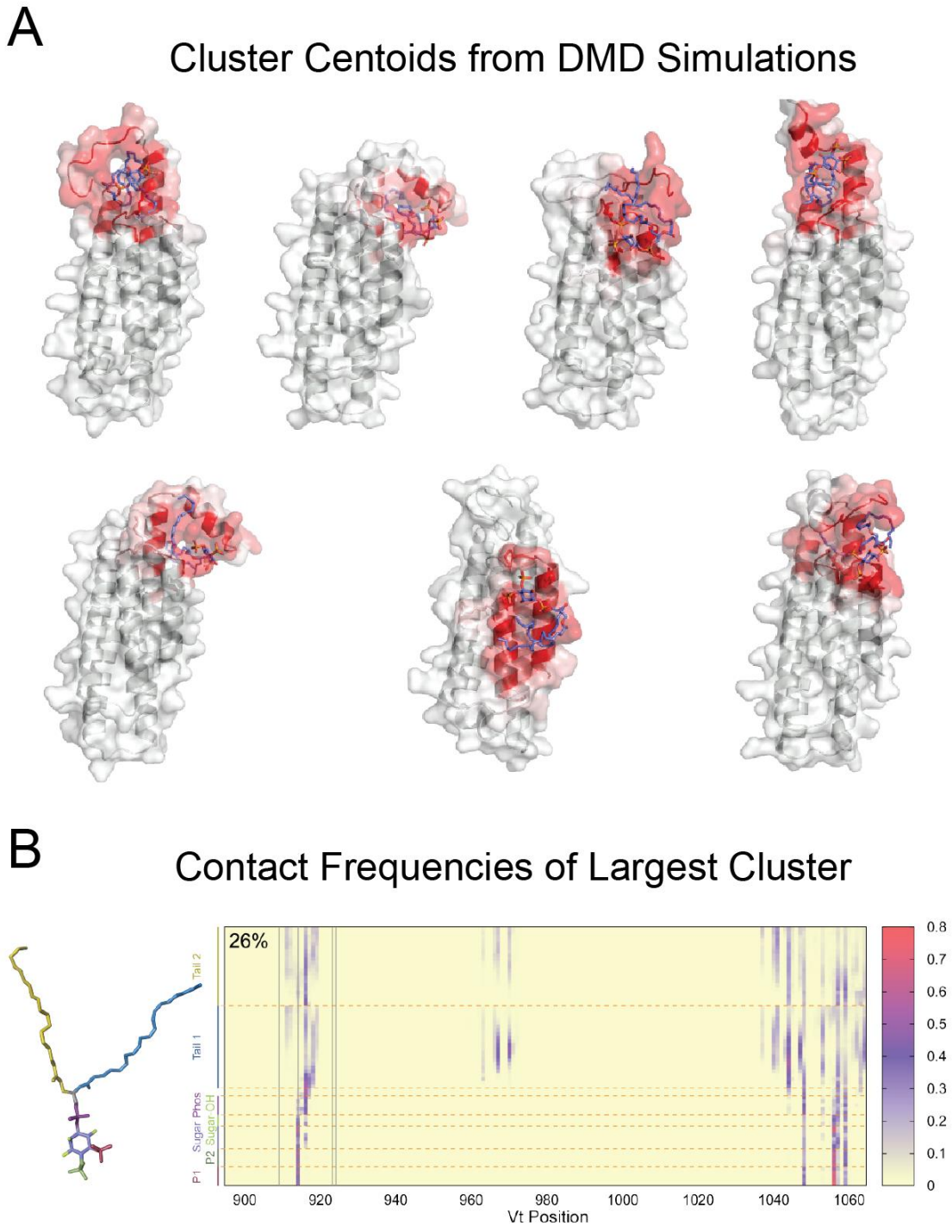

Figure S1, related to Figure 2. DMD simulations of Vt and unrestrained PIP_2.
A) Representative structures from seven clusters generated from the DMD simulation. Four of the seven clusters feature contacts between PIP_2 and basic collar. B) Heat map of contacts between Vt residues and atoms of PIP_2. Most contacts are observed between PIP_2 and the basic collar.

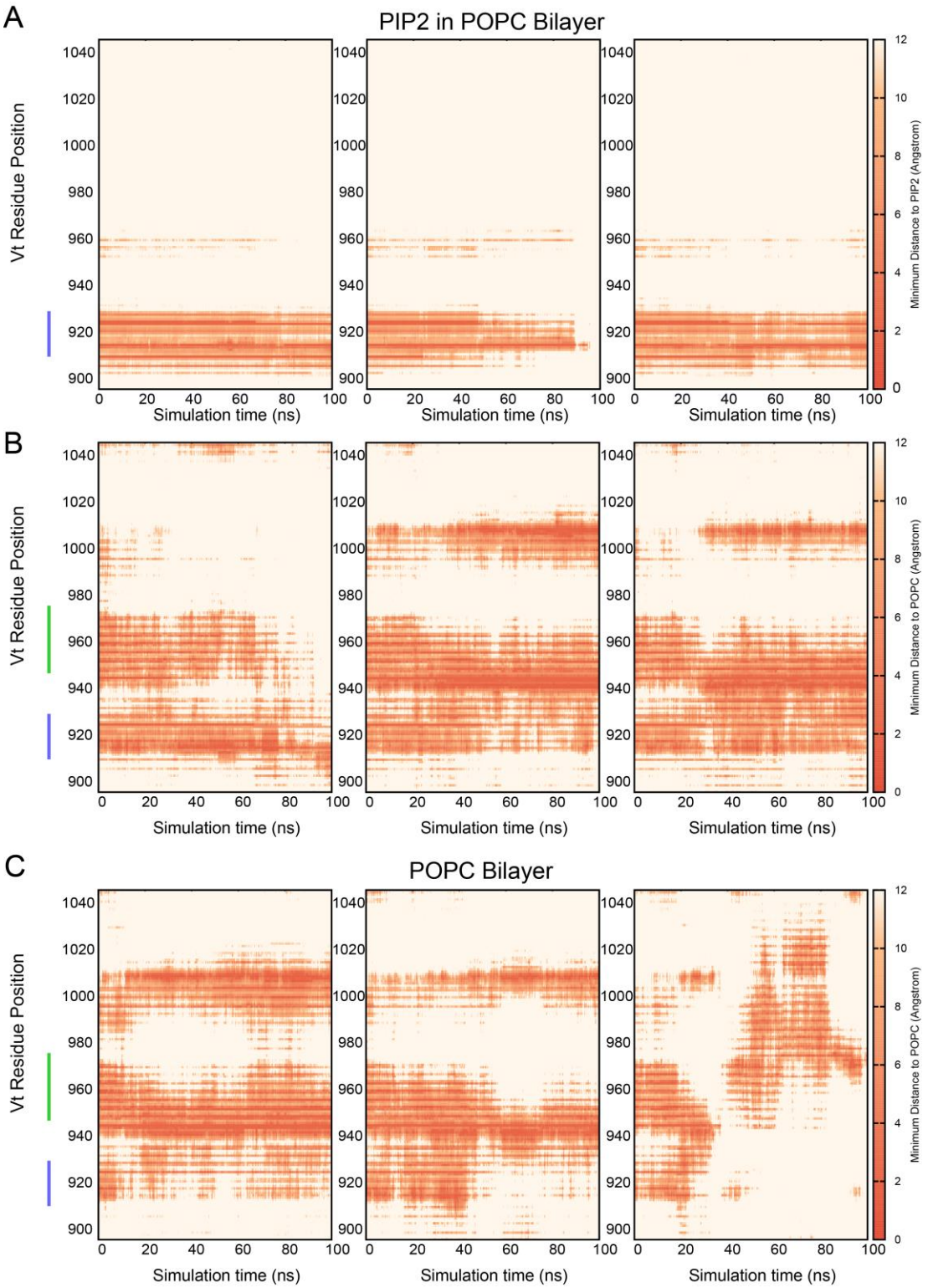

Figure S2, related to Figure 2. MD simulations of Vt in a POPC bilayer in the absence and presence of PIP_2. Heat maps displaying minimum distance between residues of Vt and (A) PIP_2 or (B) POPC, as a function of simulation time. Panel C is a heat map highlighting the minimum distance between residues of Vt and POPC in the absence of PIP_2 as a function of simulation time. The blue line marks residues of the basic collar that contact PIP_2. The green line denotes helix 3 residues. Three heat maps in each row represent three independent simulations of 100 ns each.

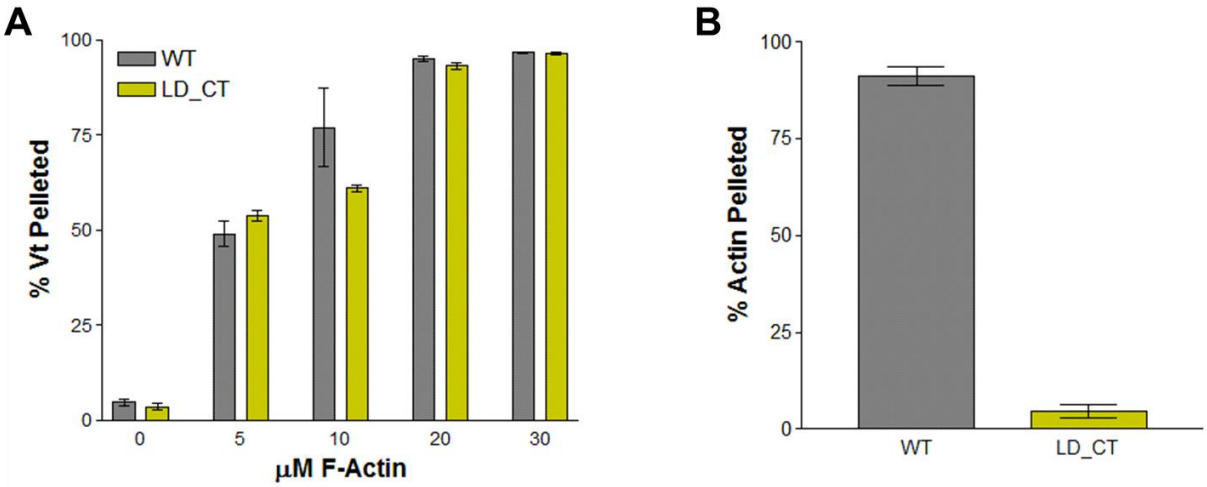

Figure S3, related to Figure 5. Actin-binding and crosslinking capacity of Vt LD-CT (R1060Q/K1061Q).

Results from actin co-sedimentation assays evaluating the ability of Vt LD-CT to bind (A) and crosslink (B) F-actin. Vt LD-CT retains F-actin binding, but is significantly impaired in its ability to crosslink F-actin. N=3, bars are ± SEM.

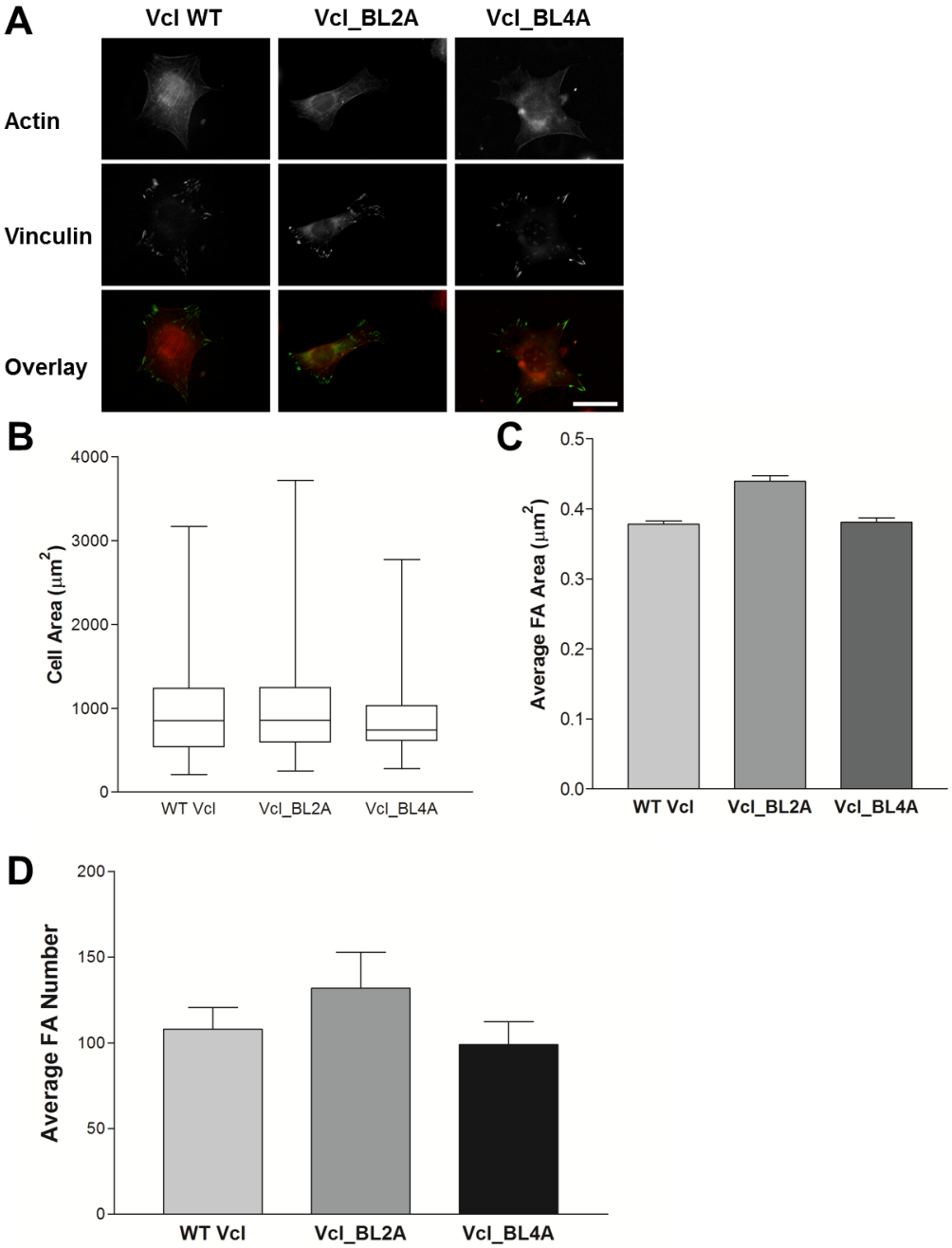

Figure S4, related to Figure 8. Lipid binding to Vcl does not alter FA size, FA number, or cellular size.

(A) Vcl -/- MEFs expressing Vcl WT, Vcl_BL2A, or Vcl_BL4A exhibit normal Vcl recruitment to FAs and do not show significant impairment in the actin cytoskeleton. Representative images are shown. Scale bar is 20 μm. (B) Vcl -/- MEFs expressing Vcl WT, Vcl_BL2A, or Vcl_BL4A are not significantly different in size. Data are represented as a box plot (n=74, 53, and 45, respectively, for Vcl WT, Vcl_BL2A, and Vcl_BL4A). (C,D) Vcl -/- MEFs expressing Vcl WT, Vcl_BL2A, or Vcl_BL4A do not exhibit significant differences in the average FA size (C) or the average number of FAs per cell (D). Data are shown as the average ± SEM (n = 53, 28, 26 cells for Vcl WT, Vcl_BL2A, and Vcl_BL4A, respectively).

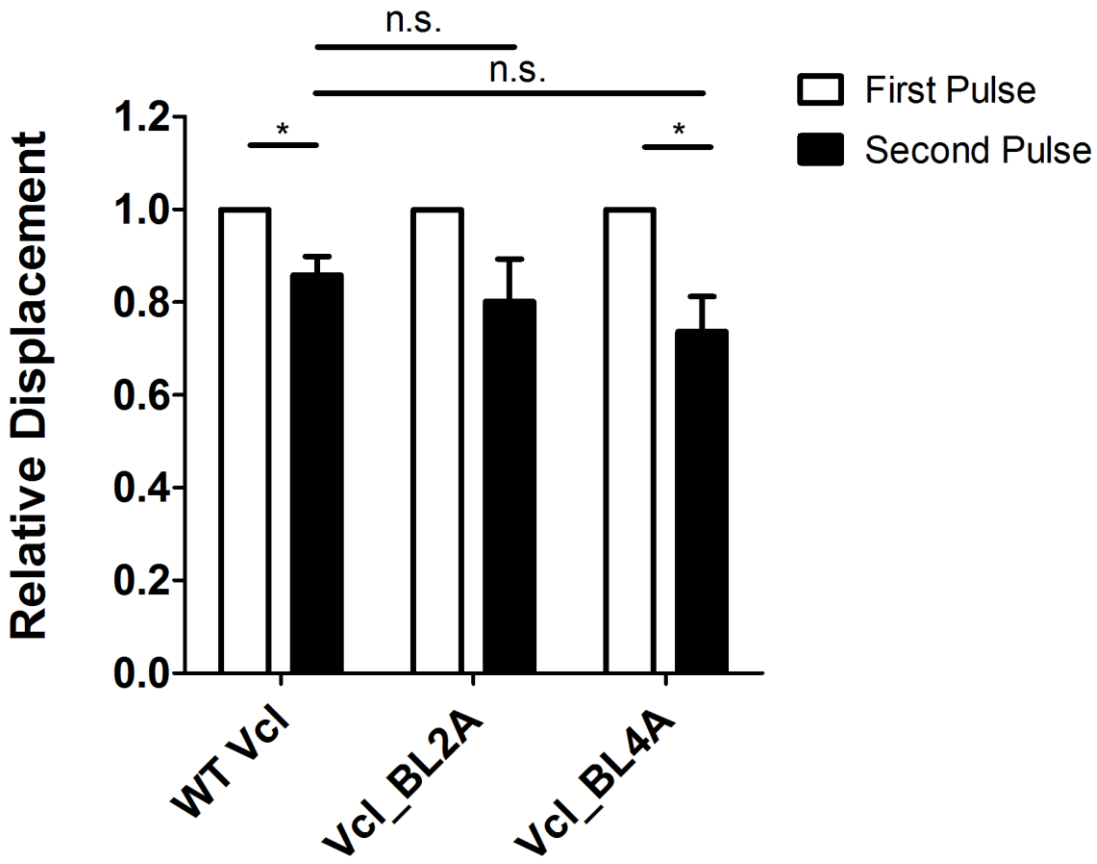

Figure S5, related to Figure 8. Lipid binding to Vcl does not alter cellular response to external forces.

3DFM experiments were used to test the reinforcement at FAs in Vcl -/- MEFs expressing Vcl constructs upon successive pulses of force. Vcl -/- MEFs expressing Vcl variants did not show significant impairment in their ability to reinforce FAs. Error bars are ± SEM (n=31, 8, 11 for Vcl WT, Vcl_BL2A, Vcl_BL4A, respectively; * for p-value < 0.01; n.s. for p > 0.05).

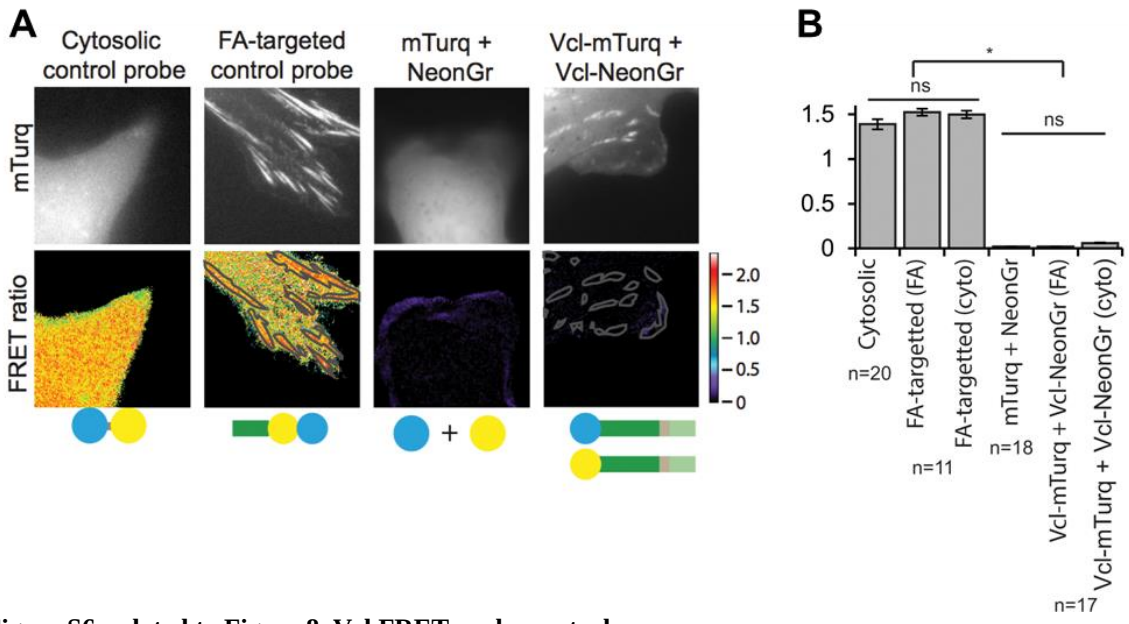

Figure S6, related to Figure 8. Vcl FRET probe controls.

Images of Vcl-/- MEFs expressing various FRET probes. (A) mTurquoise (mTurq, top) and processed mTurquoise/NeonGreen FRET ratio image (bottom) of Vcl-/- MEFs expressing various FRET probes. Cartoon schematics of the probes used are shown below the FRET images. The FA mask (grey lines) was created from the mTurq image and superimposed onto the FRET ratio image. (B) Quantification of the mean FRET ratio value in the entire cell, or inside FAs (FA) and outside FAs (Cyto). n = number of cells measured and significance is tested with ANOVA test followed by Tukey test post-hoc analysis. (* difference is significant at $p<0.05$ cutoff, ns: not significant). Error bars are ± 95% confidence intervals.

Supplemental Movies

Movie S1: Side view of 100 ns simulation of Vt interacting with a PIP_2-containing POPC bilayer, related to Figure 2.

Side view (one of three 100 ns simulations) of Vt interacting with a POPC bilayer containing PIP_2. POPC is shown in sticks with gray carbons. PIP_2 is shown as spheres with blue carbons. Vinculin is shown as a green ribbon. The time between frames is 2.5 ns.

Movie S2: Top view of 100 ns simulation of Vt interacting with a PIP_2-containing POPC bilayer, related to Figure 2.

A top-down view of the same simulation shown in Movie S1..

Movie S3: Side view of 100 ns simulation of Vt interacting with a POPC bilayer, related to Figure 2.

Side view (one the three 100 ns simulations) of Vt interacting with a POPC bilayer without PIP_2. POPC is shown in sticks with gray carbons. Vinculin is shown as a green ribbon. The time between frames is 2.5 ns.

Supplemental Experimental Procedures

Lipid co-sedimentation assays

SUVs were composed of 250 µg lipid mixture, with the reported PIP_2% using a 3:1:1 ratio of phosphatidylethanolamine:phosphatidylcholine:PS and/or PIP_2. The lipids (Avanti Polar Lipids, Alabaster, AL, USA) were resuspended by vortexing in lipid co-sedimentation buffer (40 mM MES pH 6.0, 150 mM NaCl, and 2 mM dithiotheitol (DTT)) and subsequently extruded in a mini-extruder (Avanti Polar Lipids) to produce the SUVs. Relative protein amounts were quantified using ImageJ (Abramoff et al., 2004).

Binding to PS was evaluated similarly. When assembling SUVs, the reported percentage of PS was used, and the remaining fraction of lipids contain a 3:1 mixture of phoshphatidylethanolamine:phosphatidylcholine.

Cell imaging and FA analysis

Cell imaging and FA analyses were performed as previously described (Tolbert et al., 2014). Briefly, prior to seeding, cells were serum-starved in Dulbecco's Modified Eagle Medium supplemented with 0.5% delipidated bovine serum albumin (Sigma) and antiobiotic-antimycotic solution. Cells were then resuspended in the serum-free media for approximately 2 hours before seeding onto glass coverslips coated with 50 µg/mL fibronectin (FN) for 2 hours. Cells were then fixed for 10 minutes with 3.7% formaldehyde and washed with 1X phosphate-buffered saline (PBS) followed by permeabilization for 10 minutes with 0.2% Triton X-100 in PBS and stained with phalloidin (Invitrogen, Carlsbad, CA). Coverslips were examined with a Zeiss Axiovert 200M microscope with a 63X objective lens and a Hamamatsu ORCA-ERAG digital camera. Cell area and FAs were quantified as previously reported (Shen et al., 2011). Experiments were repeated three independent times with the data represented as the mean ± SEM. Data sets were analyzed by the two-tailed Student's t test for p-values.

Force Microscopy.

Three-dimensional force microscopy (3DFM) was used to apply controlled force through magnetic beads coated with FN to engaged integrins in order to track bead displacements as a readout of cellular reinforcement. Experiments and analysis were performed as previously described (Izard et al., 2004). Bead displacements were analyzed using the two-tailed Student's t test for p-values and are reported as mean ± SEM.

Further NMR details

Chemical shift changes were tracked and chemical shift perturbations (CSP) were calculated as described (Thompson et al., 2015). To compensate for the larger chemical shift range in the ^{15}N dimension, ^{15}N chemical shifts were scaled by a factor of 9.87.

[^{15}N, ^{1}H]TRACT experiments (Lee et al., 2006) were collected using delay times of from 2 to 98 ms at 4 ms intervals. 1D spectra were integrated using Bruker Topspin software. The data were analyzed by

fitting to an exponential decay curve with a non-zero plateau. The relaxation rates were then used to calculate the effective rotational correlation times and 100 Monte Carlo simulations were used to estimate error in the calculations.

Further details of iPALM

Briefly, to use the position of the coverslip as a reference point, the measured Z-position of the coverslip was set to 0 for each imaged cell. To compare different conditions, the average Z-median, average Z-distribution and average percent of molecules in each FA layer was calculated, and 95% confidence intervals were computed by resampling the datasets 10,000 times using the Bootstrapping method. Confidence intervals are displayed as error bars on bar graphs or as lightly shaded regions on the average Z-distribution plots.

Supplemental References

Abramoff, M.D., Magalhaes, P.J., and Ram, S.J. (2004). Image Processing with ImageJ. Biophotonics International *11*, 36-42.

Izard, T., Evans, G., Borgon, R.A., Rush, C.L., Bricogne, G., and Bois, P.R. (2004). Vinculin activation by talin through helical bundle conversion. Nature *427*, 171-175.

Lee, D., Hilty, C., Wider, G., and Wuthrich, K. (2006). Effective rotational correlation times of proteins from NMR relaxation interference. J Magn Reson *178*, 72-76.

Shen, K., Tolbert, C.E., Guilluy, C., Swaminathan, V.S., Berginski, M.E., Burridge, K., Superfine, R., and Campbell, S.L. (2011). The vinculin C-terminal hairpin mediates F-actin bundle formation, focal adhesion, and cell mechanical properties. J Biol Chem *286*, 45103-45115.

Thompson, P.M., Beck, M.R., and Campbell, S.L. (2015). Protein-protein interaction analysis by nuclear magnetic resonance spectroscopy. Methods Mol Biol *1278*, 267-279.

Tolbert, C.E., Thompson, P.M., Superfine, R., Burridge, K., and Campbell, S.L. (2014). Phosphorylation at Y1065 in Vinculin Mediates Actin Bundling, Cell Spreading, and Mechanical Responses to Force. Biochemistry.